International Journal of Thermophysics, Vol. 11, No. 4, 1990

The Properties of Liquid Carbon[1]

J. Steinbeck,[2,3] G. Dresselhaus,[4] and M. S. Dresselhaus[2,5]

A model for the transport properties of liquid carbon based on Ziman liquid metal theory with refinements for polyvalent liquid metals and Fermi surface blurring is applied to calculate the electrical resistivity of liquid carbon at the melting temperature. The thermal and electrical properties predicted by the model are compared to experimental results using numerical heat flow calculations and found to be in good agreement with pulsed-current heating experiments on the resistivity of carbon fibers.

KEY WORDS: carbon (liquid); electrical resistivity; high temperatures; laser heating.

1. INTRODUCTION

The properties of the liquid phase of carbon have been of recent interest because experimental results of rapid-pulsed laser heating suggest that two different liquid phases of carbon may in fact exist [1, 2]. The properties of liquid carbon are difficult to determine by direct observation due to the extreme temperatures (>4000 K) required to melt solid carbon [3, 4], thereby forcing a reliance on indirect methods for the determination of the transport and optical properties of molten carbon. Stevenson and Ashcroft [5] have calculated the electrical resistivity of metallic liquid carbon in the

[1] Paper presented at the First Workshop on Subsecond Thermophysics, June 20–21, 1988, Gaithersburg, Maryland, U.S.A.

[2] Department of Physics, Massachusetts Institute of Technology, Cambridge, Massachusetts 02139, U.S.A.

[3] Present address: RADC/EEAC, Hanscom AFB, Massachusetts 01731, U.S.A.

[4] Francis Bitter National Magnet Laboratory, Massachusetts Institute of Technology, Cambridge, Massachusetts 02139, U.S.A.

[5] Department of Electrical Engineering and Computer Science, Massachusetts Institute of Technology, Cambridge, Massachusetts 02139, U.S.A.

0195-928X/90/0700-0789$06.00/0

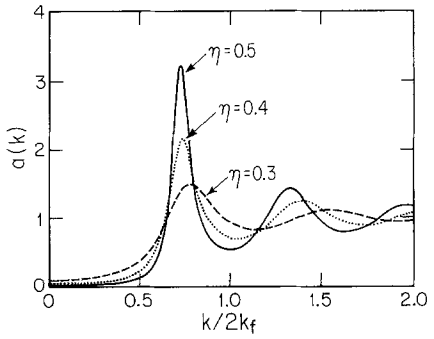

Fig. 1. Liquid structure factor for liquid carbon using the Percus–Yevick theory for packing fractions $\eta = 0.3, 0.4, 0.5$.

high-density ($>25\ \mathrm{g \cdot cm^{-3}}$) regime. In their work, the Ziman theory [6] was applied using a structure factor (see Fig. 1) for liquid carbon calculated from the Percus–Yevick theory [7], and the electrical resistivity was then calculated using the Born approximation. We have extended this model to the low-density limit and find that the predictions of this model are in good agreement with an experimental pulsed-current heating determination of the resistivity of liquid carbon [8].

2. CALCULATIONS

Recent pulsed-current melting experiments on carbon fibers indicate that liquid carbon is a liquid metal [8]. On this basis, a model for the properties of low-density liquid carbon ($1.6\ \mathrm{g \cdot cm^{-3}}$) has been constructed using Ziman liquid metal theory, which accounts for resistivity experiments on most liquid metals. The Ziman liquid metal theory requires calculation of the electron mean free path Λ from the liquid structure factor $a(k)$ and a model potential $v(k)$ for the liquid according to the relation

$$\frac{1}{\Lambda} = \left(\frac{1}{2k_f}\right) \int_0^\infty dk k^5 a(k)\, |v(k)|^2\, \Gamma(k, k_f, l) \tag{1}$$

In the conventional Ziman liquid metal theory, the Fermi surface blurring effect (discussed below) is neglected by setting $\Gamma(k, k_f, l) = 1/k$.

Of the various parameters, the electron mean free path for liquid carbon is the most sensitive to the atomic density of the liquid [9]. Experimental work by Bundy [3] provides information about the density of liquid carbon through use of the Clausius–Clapeyron relation. From Bundy's data for dp/dT and for the heat of fusion [3], the density of liquid carbon is determined to be $\sim 1.6\ \mathrm{g \cdot cm^{-3}}$.

Since liquid metals have nearly spherical Fermi surfaces, various parameters (such as the electron density n_e, the Fermi wave vector k_f, the Fermi velocity v_f, and the Fermi energy E_f) may be calculated easily on the basis of a spherical Fermi surface and the results are given in Table I [10]. We assume, as for other polyvalent liquid metals, that the electron mass is the free electron rest mass, because of a lack of detailed experimental data on the effective mass of the carriers in polyvalent liquid metals.

The liquid structure factor $a(k)$ for liquid carbon is calculated by applying the integral formula for $a(k)$ developed by Ashcroft and Lekner [7] to liquid carbon. Figure 1 shows the structure factor for liquid carbon assuming the packing fractions, $\eta = 0.3$, 0.4, and 0.5, which are typical values of η for liquid metals [7]. From Fig. 1 for the liquid structure factor, it is seen that the intensity of the primary peak increases as the packing fraction increases. This behavior is expected since as more atoms are packed into a constant volume, their positions become more rigidly fixed due to finite size effects of the atoms in the liquid.

The model potential used to calculate the transport properties of

Table I: A Summary of the Properties for the Metallic Liquid Carbon Phase [10]

Symbol	Property	Value	Model
n_e	Electron density	3.2×10^{23} cm^{-3}	4 electrons/atom
k_f	Fermi wave vector	2.1×10^{8} cm^{-1}	Fermi gas
v_f	Fermi velocity	2.45×10^{8} cm · s^{-1}	Fermi gas
E_f	Fermi energy	16.9 eV	Fermi gas
ρ_m	Mass density	1.6 g · cm^{-3}	Clausius–Clapeyron
a	Mean C–C distance	2.06 Å	—
T_m	Melting point	4450 K	Disorder depth calculation
T_v	Boiling point	4700 K	Vaporization calculation
H_f	Heat of fusion	105 kJ · mol^{-1}	Thermodynamic models
S_f	Entropy of fusion	2.63 J · mol^{-1} · K^{-1}	Thermodynamic models
ρ_l	Electrical resistivity	30 $\mu\Omega$ · cm	Pulsed-current experiments
$\kappa(T)$	Thermal conductivity	2.9 W · cm^{-1} · K^{-1}	Wiedemann–Franz
$C_p(T)$	Heat capacity	26 J · mol^{-1} · K^{-1}	Fermi gas
β_c	Compressibility	6.4×10^{-12} Pa^{-1}	Model calculation
Λ	Mean free path	3.4 Å	Ziman liquid metal model
R_f	Reflectivity	0.82	$\lambda = 694$ nm (Drude)
R_f	Reflectivity	0.7	$\lambda = 248$ nm (Drude)
α	Absorption coefficient	1.4×10^{6} cm^{-1}	$\lambda = 694$ nm (Drude)
α	Absorption coefficient	1.7×10^{6} cm^{-1}	$\lambda = 248$ nm (Drude)
D_l	Liquid diffusivity	10^{-4} cm^2 · s^{-1}	Liquid segregation model
v_p	Interface diffusive speed	26 m · s^{-1}	Liquid segregation model
k	Segregation coefficient	0.17	Liquid segregation model

liquid carbon is the Heine–Abarenkov model potential [11, 12]. Using the parameters given in Table I the model potential for liquid carbon is calculated directly. The constants A_0, A_1, and A_2 needed for calculation of the Heine–Abarenkov model potential were calculated using the energies of the carbon 3s, 3p, and 3d orbitals and tabulated values for the Coulomb wave functions [13] as reported by Animalu [14]. The constants are given by $A_0 = 2.05$, $A_1 = 2.44$, and $A_2 = 2.65$.

In Fig. 2 the model potentials calculated for carbon and silicon [14] are shown and compared for $0 < k/2k_f < 2$, illustrating the rapid decrease in the potential as k becomes smaller. Note the qualitatively similar behavior of the two potentials (for C and for Si) with the nodes at similar values of $k/2k_f$. Comparing Figs. 1 and 2 for liquid carbon, the node in the calculated model potential is seen to occur at a k value which is near the center of the primary peak in the liquid structure factor. Thus the contribution to the scattering [see Eq. (1)] will not be large even for k values where the structure factor is greatest. Initial calculations of A in liquid carbon using Eq. (1) with $\Gamma(k, k_f, l) = 1/k$ show that the mean free path is only a few interatomic spacings. Therefore, the Ziman model calculations were refined to include the blurring of the Fermi surface due to electron scattering using the Ferraz and March formula [16] for Fermi surface blurring. The results for $\Gamma(k, k_f, l)$ used in the calculation of Eq. (1) are shown in Fig. 3, where k and k_f denote the two wave vectors involved in the scattering event. In the limit $l \to \infty$ (where l is the electron mean free path for the unblurred Fermi surface model), the difference between the initial and the final k vectors cannot exceed $2k_f$.

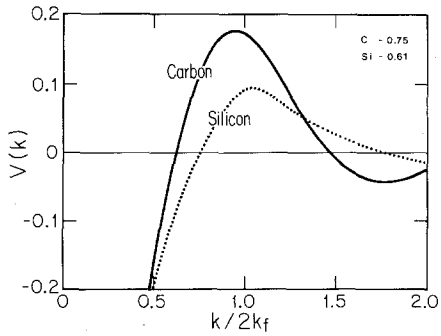

Fig. 2. The model potential (eV) for carbon compared with the model potential for Si [15] calculated using the Heine–Abarenkov model [12]. The numbers in the inset are the values of the potential at $k \to 0$.

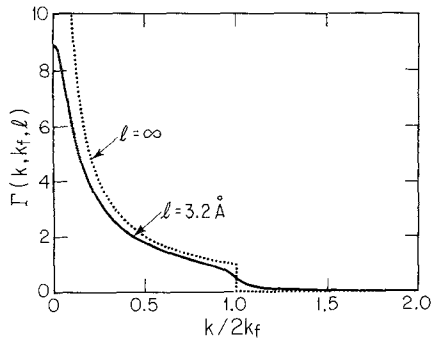

Fig. 3. The calculated functions $\Gamma(k, k_f, l \to \infty)$ and $\Gamma(k, k_f, l = 3.2\ \text{Å})$ plotted for liquid carbon illustrating the effect of a finite electron mean free path. Note that the integral for the mean free path must now be extended beyond $2k_f$.

Since the potential, $v(k)$ falls off more rapidly than k^4, the integral may be evaluated over a finite region (e.g., the first two diameters of the Fermi sphere) and a good estimate of the electron mean free path Λ is still obtained. Then evaluating the full integral in Eq. (1) by numerical techniques, we obtain for the electron mean free path for liquid carbon $\Lambda = 3.4$ Å, close to the value obtained with the simple calculation which neglected the Fermi surface blurring effect.

From the calculated Λ, the electrical resistivity of liquid carbon ρ_l immediately follows as

$$\rho_l = \frac{m v_f}{n_e e^2 \Lambda} = 39.5\ \mu\Omega \cdot \text{cm} \tag{2}$$

where we have again used the free electron gas properties [1]. This value of ρ_l compares favorably with the experimental value for the electrical resistivity of liquid carbon $\sim 30 \pm 8\ \mu\Omega \cdot \text{cm}$ [8]. It is also found that the calculated electrical resistivity is relatively insensitive to the packing density or hard-sphere radius for carbon.

Since all liquid metals can be approximately modeled as degenerate Fermi gases, we may use this fact to calculate most of the thermal properties of liquid carbon (see Table I). The specific heat of the liquid at constant pressure $C_p(T)$ is given by

$$C_p(T) = 3R + \frac{\pi^2 k_B T}{2E_f} R \tag{3}$$

where R is the gas constant. The first term on the right-hand side of Eq. (3) is the atomic contribution to $C_p(T)$, while the second term on the right-

hand side is the electronic contribution. The electronic contribution to the thermal conductivity κ can be calculated using the Wiedemann–Franz relation

$$\kappa = \frac{\pi^2 k_B^2}{3e^2} \frac{T}{\rho_l} \tag{4}$$

where ρ_l is the electrical resistivity calculated above.

The specific heat for liquid carbon has been calculated by Leider *et al.* [17] and the agreement between the liquid metal theory prediction and the prediction by Leider et al. [17] for liquid carbon agrees to within $\sim 10\%$. The temperature dependence of the specific heat in both models is linear.

The salient feature of the thermal conductivity is the large increase in the thermal conductivity when graphite melts. The thermal conductivity increases to $\sim 3\ \mathrm{W \cdot cm^{-1} \cdot K^{-1}}$ when graphite becomes molten. This value is ~ 4 times larger than the in-plane thermal conductivity of graphite at the melting temperature, while the liquid thermal conductivity is ~ 100 times the c-axis thermal conductivity of graphite at the melting temperature.

The optical properties of liquid carbon may also be calculated based on the Drude theory [9]. Using the standard relations for the dependence of the optical constants on the complex dielectric function, the reflectivity $R(\omega)$ normal to the surface and the absorption coefficient, $\alpha(\omega)$, can be calculated. See Table I for the values of $\alpha(\omega)$ and $R(\omega)$ for frequencies ω of the pulsed lasers used to melt graphite. [1]

3. DISCUSSION AND CONCLUSIONS

Since liquid carbon is a polyvalent liquid metal, the temperature dependence of the electrical resistivity is very weak for temperatures between the melting point ($T_m \sim 4450\ \mathrm{K}$) and the boiling point ($T_v \sim 4700\ \mathrm{K}$). The reason for the insensitivity to the temperature is that changes in the structure factor at low k have little effect on changing the integral in Eq. (1) since the low k values are suppressed by the k^5 weighting of the integral. Also, the primary peak in the structure factor falls close to the node in the model potential, and further, $a(k) \sim 1$ for $k > 2k_f$ so that changes in $a(k)$ do not significantly alter the results for A. The weak temperature dependence of the calculated electrical resistivity of liquid carbon is also in good agreement with the experimental measurements by Heremans et al. [8], where the temperature of the liquid carbon (superheated) is known to have gone above 5000 K, but no increase in the electrical resistivity is observed. Therefore, the temperature dependence of

$\kappa(T)$ and $C_p(T)$ for liquid carbon is given by Eqs. (3) and (4), assuming ρ_l and E_f to be constant in the temperature range between T_m and T_v.

The most convincing proof that the liquid metal model provides the correct description for liquid carbon comes when the model is tested in heat flow calculations for pulsed-laser [10] and pulsed-current [8] heating experiments. Figure 4 shows the good agreement between the resistance versus time experimental traces for pulsed current melting of two very different graphitic fibers with a numerical simulation of the experiment using the liquid metal model for liquid carbon. This particular calculation tests both the electrical resistivity and the thermal properties predicted by the calculations above.

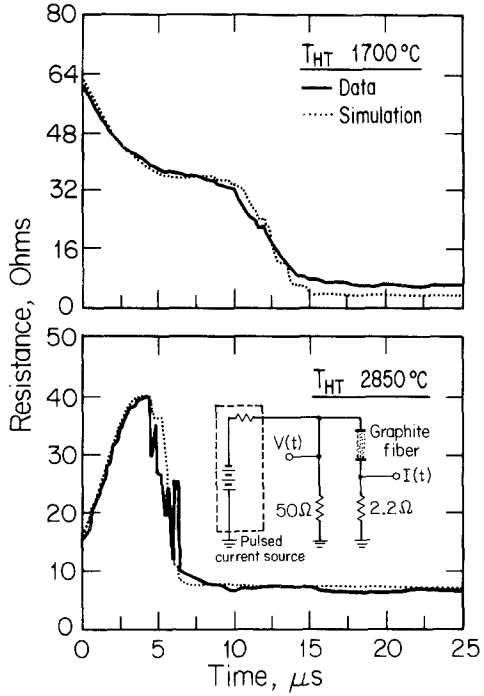

Fig. 4. Comparison of the measured (solid curve) resistance versus time traces for two carbon fibers heated by a pulsed current [8] with the corresponding traces calculated using the liquid metal model for liquid carbon. The carbon fiber with a heat treatment temperature $T_{HT} = 1700°C$ is highly disordered, while that for $T_{HT} = 2850°C$ is highly graphitic. The schematic for the experimental arrangement used to heat and melt the graphite fibers is shown in the inset to the lower trace.

Refinements to the model such as improving the model potential for atomic carbon and understanding the molecular nature of the liquid near the melting temperature may provide improved agreement with experimental results.

ACKNOWLEDGMENTS

We thank NSF Grant DMR 88–19896 for support of the work. We also thank Drs. T. Venkatesan and J. Heremans for many useful discussions.

REFERENCES

1. J. Steinbeck, G. Braunstein, M. S. Dresselhaus, T. Venkatesan, and D. C. Jacobson, *J. Appl. Phys.* **58**:4374 (1985).
2. A. M. Malvezzi, N. Bloembergen, and C. Y. Huang, *Phys. Rev. Lett.* **57**:146 (1986).
3. F. P. Bundy, *J. Chem. Phys.* **38**:618 (1963).
4. A. Cezairliyan and A. P. Miiller, *Int. J. of Thermophysics* **11**:643 (1990).
5. D. J. Stevenson and N. W. Ashcroft, *Phys. Rev. A* **9**:782 (1974).
6. J. M. Ziman, *Phil. Mag.* **6**:1013 (1961).
7. N. W. Ashcroft and J. Lekner, *Phys. Rev.* **145**:83 (1966).
8. J. Heremans, C. H. Olk, G. L. Eesley, J. Steinbeck, and G. Dresselhaus, *Phys. Rev. Lett.* **60**:452 (1988).
9. C. C. Bradley, T. E. Farber, E. G. Wilson, and J. M. Ziman, *Phil. Mag.* **7**: 865 (1962).
10. J. Steinbeck, Ph.D. thesis (Massachusetts Institute of Technology, Cambridge, 1987) (unpublished).
11. V. Heine and I. V. Abarenkov, *Phil. Mag.* **9**:451 (1964).
12. I. V. Abarenkov and V. Heine, *Phil. Mag.* **12**:529 (1966).
13. M. Blume, N. Briggs, and H. Brooks, *Tables of Coulomb Wave Functions*, Technical Report No. 260 (Cruft Laboratory, Harvard University, Cambridge, MA), 1959.
14. A. O. E. Animalu, *Phil. Mag.* **11**:379 (1965).
15. A. O. E. Animalu and V. Heine, *Phil. Mag.* **11**:1249 (1965).
16. A. Ferraz and N. H. March, *Phys. Chem. Liq.* **8**:271 (1979).
17. H. L. Leider, O. H. Krikorian, and D. A. Young, *Carbon* **11**:555 (1973).